NANO LETTERS

2008
Vol. 8, No. 2
505−510

Catalyst-Free Synthesis, Structural, and Mechanical Characterization of Twinned $Mg_2B_2O_5$ Nanowires

Xinyong Tao and Xiaodong Li*

Department of Mechanical Engineering, University of South Carolina, 300 Main Street, Columbia, South Carolina 29208

Received October 17, 2007; Revised Manuscript Received December 13, 2007

ABSTRACT

$Mg_2B_2O_5$ nanowires with (010) twins were synthesized for the first time using a catalyst-free method. The microstructure of the $Mg_2B_2O_5$ nanowires has been extensively studied by cross-sectional high-resolution transmission electron microscopy. Nanoindentation tests were performed directly on individual nanowires to probe their mechanical properties. It was found that the twinned $Mg_2B_2O_5$ nanowires achieve comparable hardness but 19% decrease in elastic modulus compared to their bulk counterpart. The elastic softening mechanisms of the $Mg_2B_2O_5$ nanowires are discussed with reference to their twin defects, size, and surface effects.

Nanostructures have attracted extraordinary attention for their fascinating potential applications.[1−4] Nanotechnology offers the ability to tailor the physical properties of nanomaterials by controlling their internal structures.[5−9] The twin boundary (TB), a significant planar defect, has important effects on the mechanical and electronic properties of materials.[9−13] Twins have been observed in Cu,[14,15] Au,[14,16] Ag,[17] Si,[18] ZnO,[19] CuO,[20] α-Fe_2O_3,[21] Zn_2SnO_4,[22] ZnS,[23] SiC,[24] GaP,[25] InP,[25] and Zn_2TiO_4[26] nanowires. To date, however, twins have not been found in metal borate nanowires.

Metal borates, a class of remarkable ceramic materials, have excellent mechanical properties, good chemical inertness, and light weight as well as low thermal expansion coefficient.[27,28] Magnesium borate has great potential in the development of thermoluminescence phosphor materials,[29] whisker-reinforced composites,[30] antiwear, and reducing friction additives.[31] Bando et al. prepared MgB_4O_7 nanowires[32] and $Mg_3B_2O_6$ nanotubes[33] via thermal evaporation and IR irradiation methods, respectively. Zhang et al. synthesized single crystalline $Mg_3B_2O_6$ nanobelts by heating a mixture of B and MgO powders under flowing Ar/H_2O gases.[34] Chang et al. reported the synthesis of $Mg_2B_2O_5$ nanowires by chemical vapor deposition method using Pt/Pd as catalyst.[27] However, developing a cost-effective technique for synthesizing $Mg_2B_2O_5$ nanowires remains a great challenge. In this work, we developed a novel catalyst-free method to synthesize $Mg_2B_2O_5$ nanowires. It is noteworthy that these nanowires have unique twinned structure. Although various techniques for synthesizing magnesium borate nanostructures have been developed, their mechanical properties are still absent. This limits their applications in constructing magnesium borate-based nanocomposites and nanodevices. Here we report for the first time to our knowledge the mechanical properties of individual $Mg_2B_2O_5$ nanowires using atomic force microscope (AFM)-based nanoindentation technique.[35,36] The twinned $Mg_2B_2O_5$ nanowires achieve comparable hardness but 19% decrease in elastic modulus compared to their bulk counterpart. These findings are significant for designing magnesium borate nanowire-based nanocomposites and functional nanodevices.

$Mg_2B_2O_5$ nanowires were synthesized via a NaCl/KCl flux method. First, 0.005 mol H_3BO_3 and 0.005 mol $MgCl_2{\cdot}6H_2O$ were dissolved in 30 mL distilled water to form a mixed solution. Then, 10 mL of 1 M NaOH solution was added dropwise into the mixed solution under ultrasonic agitation to form a white precipitate. After filtering and drying, the white precipitate was mixed uniformly with 0.003 mol boron nanoparticles (diameter = 20 nm), 0.003 mol NaCl, and 0.006 mol KCl. The mixture was then calcined in an alumina crucible at 830 °C for 2 h. The obtained powders were washed, filtered, and dried to obtain the final product.

The as-prepared powders were analyzed by X-ray diffraction (XRD). A few drops of nanowires containing ethanol solution were deposited onto copper grids or Si substrate for transmission electron microscopy (TEM, Hitachi H-8000), selected area electron diffraction (SAED), high-resolution transmission electron microscopy (HRTEM, JEOL JEM 2010F), energy dispersive X-ray spectroscopy (EDX), and nanoindentation (Hysitron, Triboscope nanoindenter) studies.

To avoid nanowire sliding during the nanoindentation tests, both ends of the nanowires to be tested were fixed through electron beam-induced deposition (EBID) of paraffin in a

* Corresponding author. E-mail: lixiao@engr.sc.edu. Web address: http://www.me.sc.edu/research/nano/.

10.1021/nl072678j CCC: $40.75
Published on Web 01/08/2008

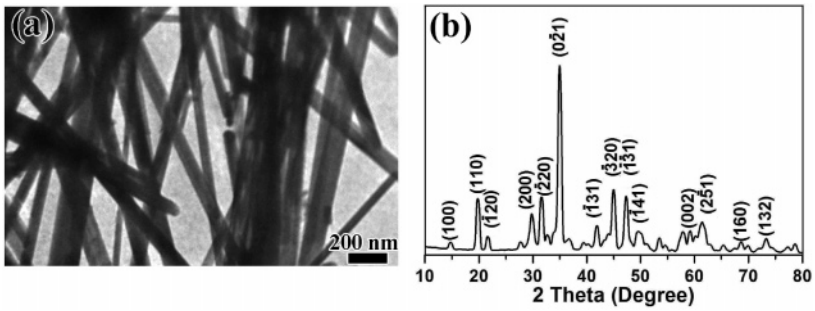

Figure 1. (a) TEM image and (b) XRD spectrum of the $Mg_2B_2O_5$ nanowires.

scanning electron microscope (SEM, FEI Quanta 200). The cross-sectional TEM specimens were prepared by slicing nanowires embedded in Spurr's epoxy resin with a Sorvall Porter-Blum MT2-B ultra microtome. For comparison, nanoindentation tests were also performed on a bulk $Mg_2B_2O_5$ (SV meteorites, Czech Republic).

A Hysitron triboscope nanoindenter in conjunction with a Veeco Dimension 3100 AFM was used to perform imaging and in situ nanoindentation tests for mechanical property measurements. The Berkovich indenter monitored and recorded the load and displacement during indentation with a force resolution of about 1 nN and displacement resolution of about 0.2 nm.[35,36] The indenter tip was first used to image and locate a single nanowire and then in situ indent the nanowire. Post-test imaging provided the ability to verify that the test was performed in the anticipated location, which maximized the reliability of data and aided in explanation of unexpected test results. Hardness and elastic modulus were calculated from the load displacement curves. Before each nanoindentation test, the thermal drift was automatically tracked and recorded by means of introducing the nanoindenter in touch with the top surface of the sample with minimum contact load. All the nanoindentation tests were performed when the thermal drift or vibration-induced mechanical drift dropped down to 0.01 nm/s. The load-displacement curves were obtained by subtracting the drift effect for hardness and elastic modulus analyses.

The TEM image in Figure 1a reveals that the product consists of abundant straight nanowires with diameter ranging from 60 to 120 nm. The surfaces of those nanowires are clean, and no amorphous coatings can be found. Figure 1b shows the XRD spectrum of the final product. All the diffraction peaks can be indexed to the suanite phase of $Mg_2B_2O_5$ (JCPDS 15−0537). No diffraction peaks from impurities were observed in the XRD spectrum, indicating high purity of the final product. In our experiments, we found that NaCl, KCl, and B powders played the key role in the synthesis of $Mg_2B_2O_5$ nanowires. The experimental results revealed that only some $Mg_3B_2O_6$ and MgO nanoparticles were obtained in the absence of NaCl, KCl, and B. $Mg_2B_2O_5$ nanoparticles and a few nanowires, instead of $Mg_3B_2O_6$, were synthesized after the addition of NaCl and KCl, and no MgO was found, indicating that NaCl and KCl can promote the reaction between MgO and B_2O_3. The addition of B nanoparticles can also affect the growth of $Mg_2B_2O_5$ nanowires. Experiments proved that NaCl, KCl, and B are all

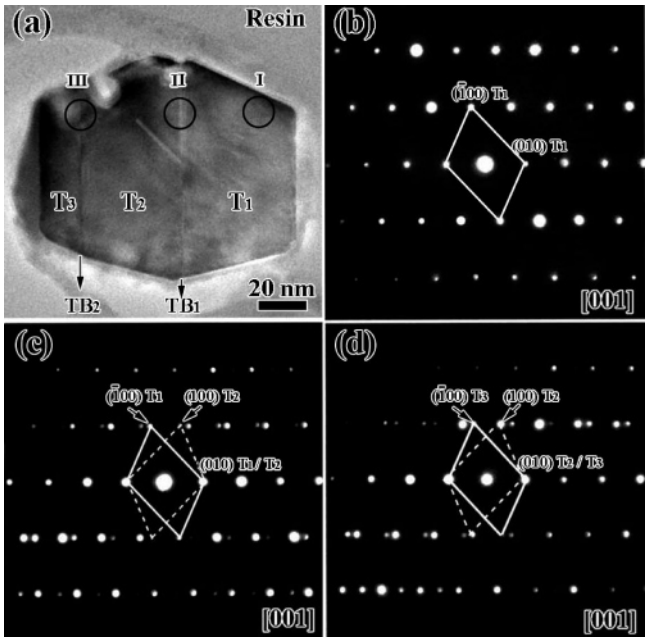

Figure 2. (a) Cross-sectional TEM image of a $Mg_2B_2O_5$ nanowire, which is composed of three building blocks T_1, T_2, and T_3. (b) SAED pattern obtained from area I. (c) SAED pattern recorded from the connection area of T_1 and T_2 (area II). (d) SAED pattern taken from the connection area of T_2 and T_3 (area III).

necessary for the growth of $Mg_2B_2O_5$ nanowires. No impurity catalyst particles were found at the ends of the $Mg_2B_2O_5$ nanowires, indicating a catalyst-free growth.

The SAED analyses showed that most of the $Mg_2B_2O_5$ nanowires had twinned structures. To obtain detailed information about the microstructure of the $Mg_2B_2O_5$ nanowires, we performed cross-sectional TEM analysis. As shown in Figure 2a, the nanowire is composed of three blocks T_1, T_2, and T_3. T_1 and T_2, T_2 and T_3 form twin structures and denote the TBs as TB_1 and TB_2, respectively. The SAED patterns taken from different blocks (T_1, T_2, and T_3) of the nanowire show similar patterns (Figure 2b) and can be indexed to the [001] zone axis. This indicates that those building blocks are single crystals with the [001] growth direction. The SAED pattern recorded from area II (TB_1) has two sets of spots with the [001] zone axis (see Figure 2c). Figure 2d shows that the SAED pattern recorded from area III (TB_2) is similar to the SAED pattern of area II. Both the SAED patterns (Figure 2, panels c and d) can be indexed as a typical rotational twinning pattern with [010] as the twin axis.

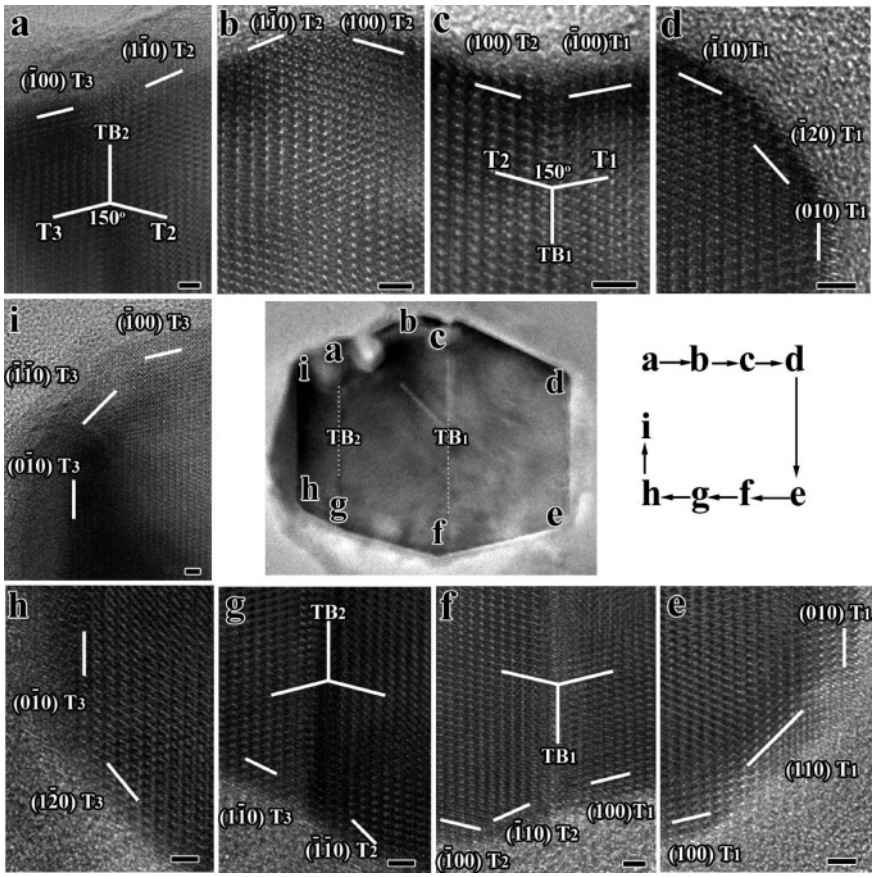

Figure 3. (a−i) Cross-sectional HRTEM images of areas a−i as indicated in the middle TEM image. All scale bars are 2 nm.

Figure 3 shows the [001] zone axis HRTEM images of different areas of a typical $Mg_2B_2O_5$ nanowire. Figure 3a is the HRTEM image recorded from part a of the cross-sectional sample. A sharp twin boundary TB_2 can be found in Figure 3a, demonstrating the well-defined twinning relationship and the well-coherent lattice across the boundary. The angle between ($\bar{1}$00) T_3 and (100) T_2 is about 150°. Two facets, ($\bar{1}$00) T_3 and (1$\bar{1}$0) T_2 appear in Figure 3a. Figure 3b reveals an obtuse angle corner formed by (1$\bar{1}$0) T_2 facet and (100) T_2 facet. Figure 3c shows another sharp twin boundary TB_1. The angle between ($\bar{1}$00) T_1 and (100) T_2 is about 150°, which is the same as that of TB_2. Interesting facets were also observed in area d, as shown in Figure 3d. A high-index facet ($\bar{1}$20) T_1 appears as the transition between the dominant facet plane ($\bar{1}$10) T_1 and (010) T_1. Figure 3e reveals a small facet (110) T_1 between (100) T_1 and (010) T_1. The other end of TB_1, which is illustrated in Figure 3f, is not as sharp as TB_1 shown in Figure 3c. This kind of extended twin boundaries exhibits few of local lattice distortion in the TB_1 vicinity. Similar lattice distortion can also be found in the vicinity of TB_2, as shown in Figure 3g. Figure 3h reveals another high-index facet (1$\bar{2}$0) T_3 in the transition between the facet (0$\bar{1}$0) T_3 and (1$\bar{1}$0) T_3. Figure 3i indicates a ($\bar{1}\bar{1}$0) T_3 facet, which is equivalent to facet (110) T_1 in atomic structure with the same surface energy.

Figure 4 shows the schematic diagram of the projected shape and facets of the $Mg_2B_2O_5$ nanowire, as illustrated in Figure 3. The polygonal plane in the cross-section provides evidence of anisotropy for lateral crystal growth. There are

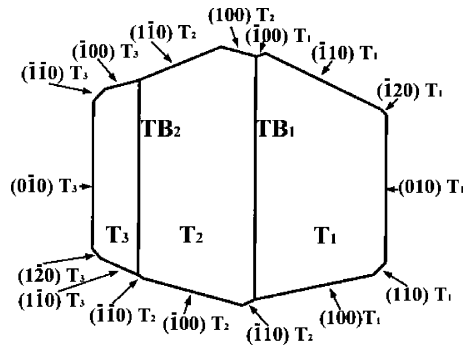

Figure 4. Schematic diagram for the projected shape and facets of the $Mg_2B_2O_5$ nanowire.

16 facets including 9 big facets and 7 small facets in this cross-sectional sample. It can be found that the low-index planes are the dominant terminating facets. Lattice planes of higher indices appeared only as transitions between the dominant facet planes of low indices. This result agrees with the lowest surface energy principle in crystal growth.

To study the mechanical properties of $Mg_2B_2O_5$ nanowires, a few drops of nanowires containing ethanol solution were deposited onto a clean Si substrate for the nanoindentation experiments. In our previous nanoindentation tests,[37−39] EBID clamping method[40] was not used to stabilize the nanostructures because there was good contact between the samples and the substrate. In this work, we found that the adhesion between magnesium borate nanowires and Si substrate was weak, which resulted from the special shapes of these

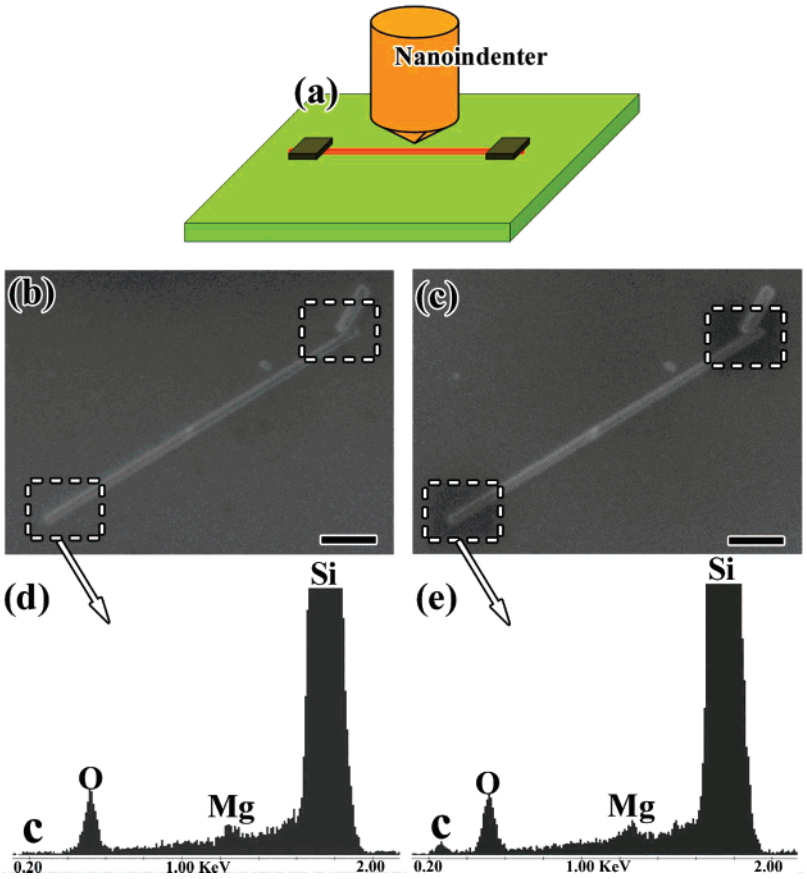

Figure 5. (a) Schematic of nanoindentation on a nanowire clamped to silicon substrate by EBID. (b,c) SEM images of a single $Mg_2B_2O_5$ nanowire before and after EBID. (d) EDX spectrum obtained from the rectangular area in panel b, showing the almost absent carbon peak before EBID, and (e) EDX spectrum obtained from the rectangular area in panel c, showing an obvious carbon peak, which indicates a carbon layer has been successfully deposited onto the rectangular area after 20 min EBID. All scale bars are 1 μm.

nanowires (see Figure 4). So the EBID clamping method was introduced to avoid the sliding of the $Mg_2B_2O_5$ nanowires. Figure 5a is the schematic of nanoindentation on a nanowire fixed to a Si substrate by EBID. Figure 5, panels b and c, shows the SEM images of a single $Mg_2B_2O_5$ nanowire before and after EBID, respectively. By examining the carbon peaks in Figure 5, panels d and e, it is clearly shown that a carbon layer has been successfully deposited at both ends of the nanowire after 20 min EBID. Some regions without carbon deposition were chosen for indentation tests. It was proved that these carbon layers were strong enough to anchor the nanowires during nanoindentation test.

Figure 6a is the three-dimensional (3D) AFM image of the EBID clamped nanowire, as illustrated in Figure 5c. The arrows highlight two EBID clamps, which are more clearly presented in the 3D AFM image. The 2D AFM image of the clamped $Mg_2B_2O_5$ nanowire is shown in Figure 6b. The insert is the corresponding cross-sectional height profile. The nanowire is about 6 μm in length and 100 nm in diameter. Panels c and d of Figure 6 reveal the representative 3D and 2D in situ AFM images of an indentation impression, respectively. The insert in Figure 6d is the cross-sectional height profile, showing the residual indentation depth is about 3.2 nm. Representative nanoindentation load-time segments and corresponding load-displacement curve are shown in Figure 6, panels e and f, respectively. The loading/unloading rate is 12.6 μN/s. The peak indentation depth in Figure 6f is 12.3 nm, which is less than 20% of the wire diameter. It is generally accepted that the depth of indentation should not exceed 30% of the particle diameter or film thickness to minimize the substrate effect.[35,36] To avoid the sample size effect on nanoindentation mechanical property measurements, the indentation contact radii were smaller than 30% of the nanowire radius.[41]

The indentation hardness and elastic modulus of $Mg_2B_2O_5$ nanowires were measured to be 15.4 ± 0.7 and 125.8 ± 3.6 GPa, respectively, obtained from twenty nanoindentation tests. Compared with bulk $Mg_2B_2O_5$ with the measured nanoindentation hardness value of 14.9 ± 0.4 GPa and an elastic modulus value of 155.4 ± 2.8 GPa, comparable hardness and 19% decrease of elastic modulus in $Mg_2B_2O_5$ nanowires can be found. The decrease in elastic modulus was also observed in other nanomaterials, such as $Al_{18}B_4O_{33}$,[28] ZnS,[39] and Au.[42,43] Many factors may lead to the reduction of elastic modulus. This decrease in elastic modulus can be attributed to the high surface-to-volume ratio of the nanowires.[39,42] Unlike the atoms locked in the lattice, surface atoms are less constrained, thereby making the nanowire easier to deform in the elastic regime and consequently leading to a lower elastic modulus.[28,39] Schaefer et al.[43] have found that the measured elastic modulus of the unannealed

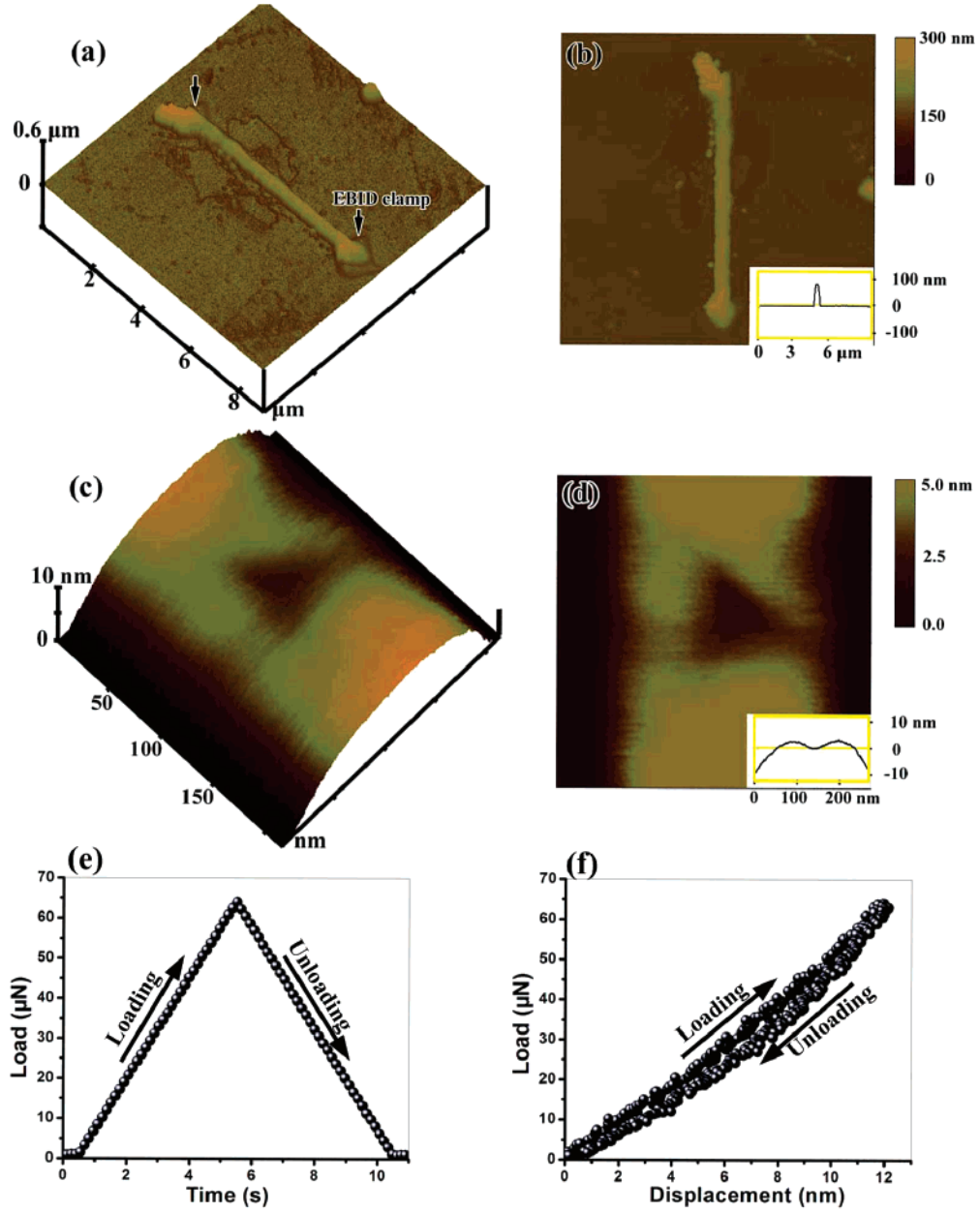

Figure 6. (a) 3D AFM image. (b) 2D AFM image of a clamped $Mg_2B_2O_5$ nanowire. The inset in panel b shows the cross-sectional height profile. (c) Representative 3D AFM image. (d) 2D AFM image of the indentation impression made on the $Mg_2B_2O_5$ nanowire shown in panel a. The inset in panel d is the cross-sectional height profile of the indentation impression. (e) Representative nanoindentation load-time segments. (f) Representative load-displacement curve.

gold nanoclusters is much lower than those of the annealed gold nanoclusters. They believed that the existence of structural defects (such as dislocations and twin boundaries) act to lower the elastic modulus of the unannealed nanoclusters. However, other papers reported that the twin structures do not affect the elastic modulus of nanomaterials but rather serve as obstacles to dislocation motion and/or as dislocation sources, which can lead to hardening effect.[9,11,14] Therefore, it is believed that the 19% decrease in elastic modulus results from the high surface-to-volume ratio (surface effect) while the slight increase in hardness results from the twin structure. Because only few twin boundaries exist in individual $Mg_2B_2O_5$ nanowires, the hardness increase is not significant. By controlling the types and number of twin structures, we should be able to improve and/or tailor the strength of nanomaterials.

In summary, we synthesized $Mg_2B_2O_5$ nanowires via a catalyst-free method. It was found that NaCl, KCl, and boron played the key role in the growth of the nanowires. HRTEM and SAED studies showed that the nanowires had twinned structures with the growth direction along [001]. The hardness and elastic modulus were measured by directly indenting individual EBID fixed nanowires. Those $Mg_2B_2O_5$ nanowires exhibit hardness of 15.4 ± 0.7 GPa and elastic modulus of 125.8 ± 3.6 GPa. Compared with bulk $Mg_2B_2O_5$, the hardness of the nanowires is comparable while the elastic

modulus is decreased approximately by 19%. These findings are significant for designing magnesium borate nanowire-based nanocomposites and nanodevices.

Acknowledgment. Financial support for this study was provided by the National Science Foundation (CMMI-0653651 and EPS-0296165), the ACS Petroleum Research Fund (ACS PRF 40450-AC10), and the University of South Carolina NanoCenter. We thank Douglas Blom and Soumitra Ghoshroy (the University of South Carolina EM Center) for TEM technical support.

References

(1) Yang, P. D.; Lieber, C. M. *Science* **1996**, *273*, 1836.
(2) Xiang, J.; Lu, W.; Hu, Y.; Wu, Y.; Yan, H.; Lieber, C. M. *Nature* **2006**, *441*, 489.
(3) Wang, X. D.; Song, J. H.; Liu, J.; Wang, Z. L. *Science* **2007**, *316*, 102.
(4) Yip, S. *Nat. Mater.* **2007**, *3*, 11.
(5) Fan, H. Y.; Hartshorn, C.; Buchheit, T.; Tallant, D.; Assink, R.; Simpson, R.; Kisse, D. J.; Lacks, D. J.; Torquato, S.; Brinker, C. J. *Nat. Mater.* **2007**, *6*, 418.
(6) Wang, Z. W.; Daemen, L. L.; Zhao, Y. S.; Zha, C. S.; Downs, R. T.; Wang, X. D.; Wang, Z. L.; Hemley, R. J. *Nat. Mater.* **2005**, *4*, 922.
(7) Schiotz, J.; Jacobsen, K. W. *Science* **2003**, *301*, 1357.
(8) Wiley, B. J.; Xiong, Y. J.; Li, Z. Y.; Yin, Y. D.; Xia, Y. N. *Nano Lett.* **2006**, *6*, 765.
(9) Lu, L.; Shen, Y. F.; Chen, X. H.; Qian, L. H.; Lu, K. *Science* **2004**, *304*, 422.
(10) Bietsch, A.; Michel, B. *Appl. Phys. Lett.* **2002**, *80*, 3346.
(11) Cao, A. J.; Wei, Y. G.; Mao, S. X. *Appl. Phys. Lett.* **2007**, *90*, 151909.
(12) Wang, J.; Huang, H. C. *Appl. Phys. Lett.* **2006**, *88*, 203112.
(13) Afanasyev, K. A.; Sansoz, F. *Nano Lett.* **2007**, *7*, 2056.
(14) Wang, J. G.; Tian, M. L.; Mallouk, T. E.; Chan, M. H. W. *J. Phys. Chem. B* **2004**, *108*, 841.
(15) Toimil-Molares, M. E.; Buschmann, V.; Dobrev, D.; Neumann, R.; Scholz, R.; Schuchert, I. U.; Vetter, J. *Adv. Mater.* **2001**, *13*, 62.
(16) Tian, M. L.; Wang, J. U.; Kurtz, J.; Mallouk, T. E.; Chan, M. H. W. *Nano Lett.* **2003**, *3*, 919.
(17) Wu, B.; Heidelberg, A.; Boland, J. J.; Sader, J. E.; Sun, X. M.; Li, Y. D. *Nano Lett.* **2006**, *6*, 468.
(18) Carim, A. F.; Lew, K. K.; Redwing, J. M. *Adv. Mater.* **2001**, *13*, 1489.
(19) Zhang, Z. H.; Liu, H. H.; Jian, J. K.; Zou, K.; Duan, X. F. *Appl. Phys. Lett.* **2006**, *88*, 193101.
(20) Jiang, X. C.; Herricks, T.; Xia, Y. N. *Nano Lett.* **2002**, *2*, 1333.
(21) Wang, R. M.; Chen, Y. F.; Fu, Y. Y.; Zhang, H.; Kisielowski, C. *J. Phys. Chem. B* **2005**, *109*, 12245.
(22) Chen, H. Y.; Wang, J. X.; Yu, H. C.; Yang, H. X.; Xie, S. S.; Li, J. Q. *J. Phys. Chem. B* **2005**, *109*, 2573.
(23) Meng, X. M.; Jiang, Y.; Liu, J.; Lee, C. S.; Bello, I.; Lee, S. T. *Appl. Phys. Lett.* **2003**, *83*, 2244.
(24) Wu, R. B.; Pan, Y.; Yang, G. Y.; Gao, M. X.; Wu, L. L.; Chen, J. J.; Zhai, R.; Lin, J. *J. Phys. Chem. C* **2007**, *111*, 6233.
(25) Xiong, Q. H.; Wang, J.; Eklund, P. C. *Nano Lett.* **2006**, *6*, 2736.
(26) Yang, Y.; Sun, X. W.; Tay, B. K.; Wang, J. X.; Dong, Z. L.; Fan, H. M. *Adv. Mater.* **2007**, *19*, 1839.
(27) Li, Y.; Fan, Z. Y.; Lu, J. G.; Chang, R. P. H. *Chem. Mater.* **2004**, *16*, 2512.
(28) Tao, X. Y.; Wang, X. N.; Li, X. D. *Nano Lett.* **2007**, *7*, 3172.
(29) Shahare, D. I.; Dhoble, S. J.; Moharil, S. V. *J. Mater. Sci. Lett.* **1993**, *12*, 1873.
(30) Wu, P. L.; Tian, Z.; Wang, L. D.; Fei, W. D. *Thermochim. Acta* **2007**, *455*, 7.
(31) Hu, Z. S.; Lai, R.; Lou, F.; Wang, L. G.; Chen, Z. L.; Chen, G. X.; Dong, J. X. *Wear* **2002**, *252*, 370.
(32) Ma, R. Z.; Bando, Y.; Sato, T. *Appl. Phys. Lett.* **2002**, *81*, 3467.
(33) Ma, R. Z.; Bando, Y.; Golberg, D.; Sato, T. *Angew. Chem., Int. Ed.* **2003**, *42*, 1836.
(34) Zhang, J.; Li, Z. Q.; Zhang, B. *Mater. Chem. Phys.* **2006**, *98*, 195.
(35) Li, X. D.; Bhushan, B. *Mater. Charact.* **2002**, *48*, 11.
(36) Bhushan, B.; Li, X. D. *Int. Mater. Rev.* **2003**, *48*, 125.
(37) Li, X. D.; Gao, H. S.; Murphy, C. J.; Caswell, K. K. *Nano Lett.* **2003**, *3*, 1495.
(38) Li, X. D.; Gao, H. S.; Murphy, C. J.; Gou, L. F. *Nano Lett.* **2004**, *4*, 1903.
(39) Li, X. D.; Wang, X. N.; Xiong, Q. H.; Eklund, P. C. *Nano Lett.* **2005**, *5*, 1982.
(40) Ding, W.; Dikin, D. A.; Chen, X.; Piner, R. D.; Ruoff, R. S.; Zussman, E.; Wang, X. N.; Li, X. D. *J. Appl. Phys.* **2005**, *98*, 014905.
(41) Xu, Z. H.; Li, X. D. *Acta Mater.* **2006**, *54*, 1699.
(42) Hu, M.; Hillyard, P.; Hartland, G. V.; Kosel, T.; Perez-Juste, J.; Mulvaney, P. *Nano Lett.* **2004**, *4*, 2493.
(43) Schaefer, D. M.; Patil, A.; Andres, R. P.; Reifenberger, R. *Phys. Rev. B* **1995**, *51*, 5322.

NL072678J